# Three-dimensional microfluidic model for tumor cell intravasation and endothelial barrier function

Ioannis K. Zervantonakis[a], Shannon K. Hughes-Alford[b,c], Joseph L. Charest[d], John S. Condeelis[e], Frank B. Gertler[c], and Roger D. Kamm[a,b,1]

[a]Departments of Mechanical Engineering, [b]Biological Engineering, and [c]Koch Institute for Integrative Cancer Research, Massachusetts Institute of Technology, Cambridge, MA 02139; [d]The Charles Stark Draper Laboratory, Cambridge, MA 02139; and [e]Department of Anatomy and Structural Biology, Albert Einstein College of Medicine, Bronx, NY 10461

Edited by David A. Weitz, Harvard University, Cambridge, MA, and approved July 10, 2012 (received for review June 18, 2012)

**Entry of tumor cells into the blood stream is a critical step in cancer metastasis. Although significant progress has been made in visualizing tumor cell motility in vivo, the underlying mechanism of cancer cell intravasation remains largely unknown. We developed a microfluidic-based assay to recreate the tumor-vascular interface in three-dimensions, allowing for high resolution, real-time imaging, and precise quantification of endothelial barrier function. Studies are aimed at testing the hypothesis that carcinoma cell intravasation is regulated by biochemical factors from the interacting cells and cellular interactions with macrophages. We developed a method to measure spatially resolved endothelial permeability and show that signaling with macrophages via secretion of tumor necrosis factor alpha results in endothelial barrier impairment. Under these conditions intravasation rates were increased as validated with live imaging. To further investigate tumor-endothelial (TC-EC) signaling, we used highly invasive fibrosarcoma cells and quantified tumor cell migration dynamics and TC-EC interactions under control and perturbed (with tumor necrosis factor alpha) barrier conditions. We found that endothelial barrier impairment was associated with a higher number and faster dynamics of TC-EC interactions, in agreement with our carcinoma intravasation results. Taken together our results provide evidence that the endothelium poses a barrier to tumor cell intravasation that can be regulated by factors present in the tumor microenvironment.**

cancer migration | transmigration | cancer–endothelial cell interactions | in vitro | 3D microfluidics

Tumor-endothelial cell interactions are critical in multiple steps during cancer metastasis, ranging from cancer angiogenesis to colonization. Cancer cell intravasation is a rate-limiting step in metastasis that regulates the number of circulating tumor cells and thus presents high risk for the formation of secondary tumors (1, 2). During the metastatic process tumor cells migrate out of the primary tumor (3), navigate into a complex tumor microenvironment, and enter into blood vessels (4). Cell-cell communication and chemotaxis (5) are key to this process and can occur via paracrine signals and/or direct contact between different cell types during tumor cell invasion (6) and metastatic colonization (7). Studies using multiphoton imaging in animal models have demonstrated that the ability of tumor cells to enter into the blood stream can be controlled both by tumor cell intrinsic factors (8–11) and other cells present in the tumor microenvironment, such as macrophages (12) and neutrophils (13). However, because of the lack of physiologically relevant in vitro models and the challenges of investigating cell-cell interactions in vivo, the underlying mechanism of intravasation remains poorly understood (14). In particular, a number of fundamental questions remain as to whether intravasation is an active or passive process (15) and whether tumor cells cross the endothelial barrier through cell-cell junctions (paracellular) or through the endothelial cell body [transcellular (16)]. Therefore, the development of experimental platforms enabling real-time visualization of tumor cell interactions with a vascular interface will enable studies for delineating the underlying molecular mechanisms, whereas these tools could also be used for drug screening and discovery.

Tumor blood vessels are highly heterogeneous, hyperpermeable, and become abnormal early during carcinogenesis (17). Despite progress in characterizing these vessels (18, 19), it is not clear whether tumor cells require abnormal blood vessels to intravasate and how tumor cells and other factors in the tumor microenvironment (e.g., macrophages) contribute to vessel remodeling. Although in vivo imaging studies in animals have demonstrated the highly dynamic interaction between tumor and endothelial cells (9, 10, 12, 20), quantitation of, or control over, vessel permeability and tumor microenvironmental factors is challenging. On the other hand, studies employing transwell inserts (21) that allow for manipulation of tumor-endothelial interactions do not enable visualization of intravasation events in real-time or precise control over cell-cell distance and growth-factor gradients. Progress in microfluidic technology has enabled the development of in vitro assays that facilitate the study of cellular behavior under tightly controlled microenvironments with high spatiotemporal resolution. Hence, modeling the tumor microenvironment by integrating the interactions among multiple cell types with biochemical and biophysical factors is a very attractive target for microfluidics. Toward this end, a number of microfluidic designs have been developed to study growth-factor gradients in cancer cell migration (22, 23), tumor-stromal cell interactions (24), and tumor-endothelial cell interactions (25).

We present an in vitro three-dimensional (3D) microfluidic model of the tumor-vascular interface designed to integrate live imaging, precise control of microenvironmental factors, and endothelial barrier measurement. In this study, we employ our model to explore the relationship between tumor cell intravasation and endothelial permeability in the context of cytokine-induced endothelial cell activation and paracrine signaling loops involving macrophages and tumor cells. Increases in endothelial permeability via signaling with macrophages or stimulation with tumor necrosis factor alpha (TNF-α) were associated with a higher intravasation rate. Blocking macrophage-secreted TNF-α reduced the intravasation rate and normalized endothelial barrier integrity. Furthermore, modulation of endothelial barrier function regulated the number and dynamics of tumor-endothelial cell interaction events. Interestingly, macrophage M1/M2 polarization status in the device during signaling with tumor and endothelial cells was similar to the macrophage monoculture conditions. These results demonstrate the utility of our microfluidic-

Author contributions: I.K.Z., J.L.C, and R.D.K., designed research; I.K.Z. performed research; S.K.H.-A. and F.B.G. contributed new reagents; I.K.Z. analyzed data; and I.K.Z., S.K.H.-A., J.L.C, J.S.C., and R.D.K. wrote the paper.

The authors declare no conflict of interest.

This article is a PNAS Direct Submission.

[1]To whom correspondence should be addressed. E-mail: rdkamm@mit.edu.

This article contains supporting information online at www.pnas.org/lookup/suppl/doi:10.1073/pnas.1210182109/-/DCSupplemental.

based approach for direct observation of different tumor cell phenotypes and heterotypic cell-cell interactions during intravasation, and provide evidence for the interplay between endothelial barrier function and tumor cell intravasation.

## Results

**Design of the 3D Tumor-Endothelial Intravasation Microfluidic-Based Assay.** The microfluidic assay consists of two independently addressable microchannels (Fig. 1*A*), where tumor and endothelial cells are seeded. These two channels are interconnected via a 3D ECM hydrogel, which includes 37 regions (Fig. 1*B*) enabling multiple simultaneous observations. The tumor cells invade in 3D in response to externally applied growth-factor gradients [e.g., epidermal growth factor (EGF) (26, 27)] or paracrine signals by the endothelial cells or other stromal cell types [e.g., macrophages (28, 29)]. On the 3D ECM-endothelial channel interface, a continuous endothelial monolayer is formed, which enables the observation of intravasation across a hollow vascular lumen, and allows for access to the basal and apical endothelial surfaces through the microchannels. Another important advantage compared to two-dimensional and transwell assays, is the introduction of a 3D matrix, which allows for both paracrine and juxtacrine signaling between tumor and endothelial cells.

To demonstrate the formation of confluent, 3D endothelial barriers (Fig. 1*C*), we visualized the endothelial cell-cell junctions using a vascular endothelial-cadherin (VE-cadherin) antibody. The endothelial cells formed continuous cell-cell junctions spanning the full area of the microchannel surfaces and the 3D ECM-endothelial channel interface (Fig. 1*C*). These confluent endothelial monolayers formed in the presence of invading tumor cells in 3D (Fig. 1*D*). High-resolution imaging allowed us to monitor endothelial cell-cell cadherin junctions as the tumor cells invaded toward the endothelial monolayer (Fig. 1*E*) and contacted the endothelial cells (Fig. 1*F*).

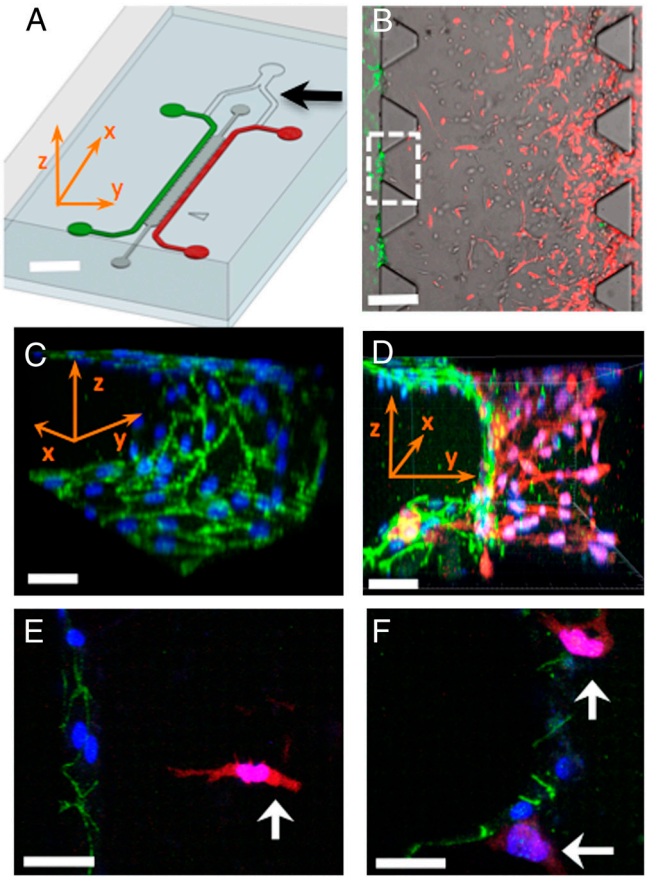


**Fig. 1.** Microfluidic tumor-vascular interface model. (*A*) Endothelial channel (green), tumor channel (red), and 3D ECM (dark gray) between the two channels. Channels are 500 μm wide, 20 mm in length, and 120 μm in height. Black arrow shows the *y*-junction. (Scale bar: 2 mm.) (*B*) Phase contrast image showing the fibrosarcoma cells (HT1080, red) invading through the ECM (gray) toward the endothelium (MVEC, green). A single 3D ECM hydrogel matrix region is outlined with the white dashed square. (Scale bar: 300 μm.) (*C*) VE-cadherin and DAPI staining to show the confluency of the endothelial monolayer on the 3D ECM (outlined with white square in *B*). (*D*) Three-dimensional rendering of a confocal *z*-stack of a single region showing the tumor cells invading in 3D and adhering to the endothelium. (Scale bar: 30 μm.) (*E*) HT1080 cell (white arrow) invading in 3D toward the endothelium. (Scale bar: 30 μm.) (*F*) HT1080 cells in contact with the endothelial monolayer. In *C*–*F* all scale bars are 30 μm. Green, VE-cadherin; blue, DAPI; red, HT1080-mCherry. *x*-, *y*-, *z*- coordinate indication is appropriately adjusted in *A*, *C*, and *D*.

**Characterization of Endothelial Monolayer Barrier Function.** Using fluorescence conjugated dextran we established a diffusion-based solute flux across the endothelial monolayer (Fig. 2*A*) that was used to measure the diffusive endothelial permeability ($P_D$). Detailed computational modeling (Fig. 2*B*) based on device geometry and measured permeability coefficients predicted the experimental concentration distribution, thus confirming the validity of our quantification framework. By monitoring the intensity profiles (Fig. 2*C*) in time, we could also measure the temporal response of the endothelium to biochemical factors (Fig. S1). $P_D$ was measured in the presence of tumor cells for 10 and 70 kDa dextrans, yielding values of $4.08 \pm 1.11 \times 10^{-5}$ cm/s and $0.75 \pm 0.093 \times 10^{-5}$ cm/s, respectively. The ratio of 10 to 70 kDa $P_D$ values was 5.5 (Fig. 2*D*), indicating that the endothelial monolayer within our devices forms a size-selective barrier for transendothelial transport.

**Macrophages Regulate Tumor Cell Intravasation Across the Endothelium.** To model a physiologically relevant intravasation phenotype, we seeded human breast carcinoma cells in the 3D matrix and

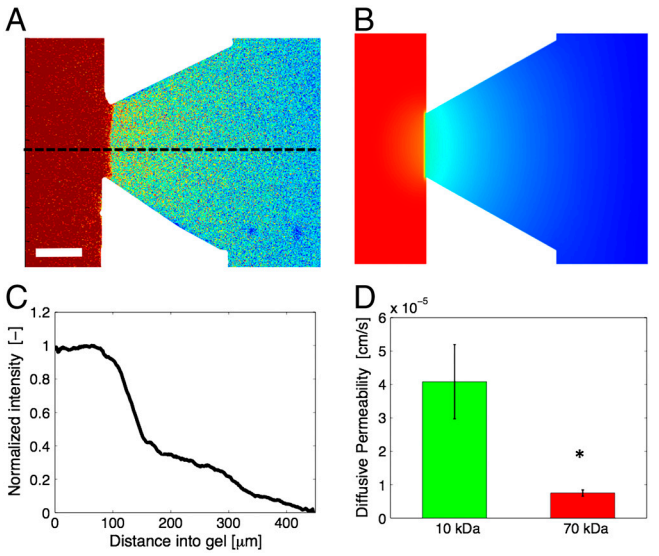


**Fig. 2.** Characterization of endothelial permeability. (*A*) Single confocal slice showing the distribution of a 10 kDa fluorescent dextran in a 3D hydrogel ECM region. Warmer colors indicate higher fluorescent intensities. (Scale bar: 50 μm.) (*B*) Computational simulation of biomolecular transport under the experimental conditions of *A*. (*C*) Normalized fluorescent intensity profile along the dashed line in *A* illustrating the sharp drop of dextran concentration across the endothelial monolayer and the steady diffusive flux inside the 3D ECM. (*D*) Diffusive permeability ($P_D$) of endothelial monolayer (MVEC) in the presence of tumor cells (HT1080) for 10 and 70 kDa dextrans. Average values across $n = 10$ regions within a single device; error bars represent SEM ($P = 0.013$). Fluorescence intensity in *C* was normalized with respect to the value at the starting point of the dashed line in *A*.

investigated whether the presence of macrophages in contact with the endothelium regulates intravasation. Intravasation is indicated by the migration of tumor cells from within the 3D matrix across the basal endothelial surface and subsequent appearance on the apical endothelial surface inside the vascular lumen. Fig. 3*A*, demonstrates a characteristic example of an intravasation event, where the breast tumor cell has adhered to the apical surface of the endothelium, as shown by the top and side views. In the absence of macrophages, tumor cells were observed predominantly on the basal side of the endothelial monolayer (Fig. 3*B*). This finding was also confirmed by quantifying the tumor cell numbers in contact with the endothelium (Fig. S2*A*) and was further validated by live cell imaging, (Fig. 3*C* and Movie S1). Intravasation was a rare and inefficient event and occurred for a small fraction of the tumor cells in contact with the endothelial monolayer. In the presence of macrophages a significantly ($P = 0.048$) higher percentage of tumor cells ($4.08 \pm 0.87\%$; 13 out of 289 cells) intravasated, compared to control conditions ($0.45 \pm 0.28\%$; 2 out of 304 cells), i.e., a ninefold increase (Fig. 3*D*). Furthermore, we showed that macrophages enabled tumor cell intravasation for endothelial cells of different origin, and that the percentage of tumor cells that had intravasated

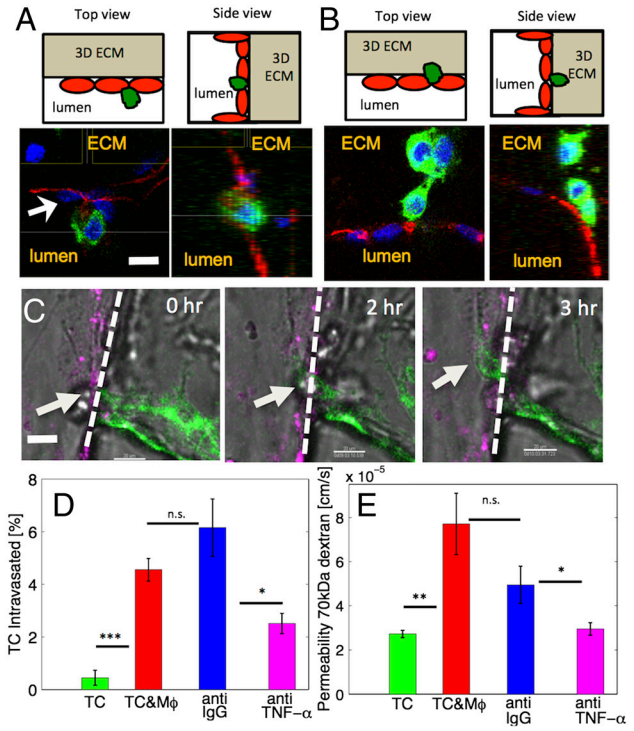


**Fig. 3.** Macrophages enable tumor cell intravasation. (*A*) *Top* (*Upper Left*) and side (*Upper Right*) views showing the device schematic with the endothelial monolayer, the tumor cells, and the location of the 3D ECM. (*Lower*) Confocal images, demonstrating intravasation of a single breast carcinoma cell (green) across the endothelium (MVEC, stained red for VE-cadherin). (Scale bar: 30 μm.) (*B*) *Top* (*Upper Left*) and side (*Upper Right*) views with the same orientation as in *A*, showing tumor cells on the basal side of the endothelium. (*C*) Time sequence of a single confocal slices showing a breast carcinoma cell (white arrow) in the process of intravasaton across a HUVEC monolayer (magenta) in the presence of macrophages (RAW264.7). The dashed line illustrates the endothelial-ECM interface. (Scale bar: 30 μm.) (*D*) Percentage of carcinoma cells that intravasated across a HUVEC monolayer was increased in the presence of macrophages (M$\varphi$, $P = 6 \times 10^{-4}$). Blocking TNF-α resulted in a significant reduction in intravasation compared to the IgG antibody control ($P = 0.035$). Average values ($n = 3$ devices) for each condition. (*E*) Quantification of endothelial permeability to 70 kDa dextrans. Presence of macrophage led to significant permeability increase ($P = 0.002$). TNF-α blocking also resulted in a significant reduction ($P = 0.036$) compared to the IgG antibody control. Average values ($n = 12$ regions); error-bars represent SEM.

(Fig. S2*B*) was similar for human microvascular endothelial (MVEC) and human umbilical vein endothelial (HUVEC) cells. To examine the effects of macrophages on the endothelial monolayer, we monitored changes in endothelial barrier function and measured a statistically significant ($P = 0.03$) 2.83-fold increase in endothelial diffusive permeability to 70 kDa dextran (Fig. 3*E*). Macrophages were present in both the subluminal and luminal endothelial spaces (Fig. S2*C*) at similar numbers ($6.42 \pm 1.88$ vs. $5.29 \pm 1.00$ cells/region, $P = 0.61$).

**TNF-α Stimulation of Endothelial Monolayer Modulates Tumor Cell Intravasation, Tumor-Endothelial Cell Interactions, and Endothelial Barrier Function.** To test the hypothesis that the macrophage-induced permeability increase results in higher intravasation rates, we perturbed the endothelial barrier using biochemical factors and measured intravasation rates. We modulated endothelial permeability by stimulation of the endothelial monolayer with 2 ng/mL TNF-α in the presence of breast carcinoma cells alone, while simultaneously establishing a 20 ng/mL per mm EGF gradient to guide carcinoma cells toward the endothelial channel. We observed a significantly ($P = 0.034$) higher number (9 out of 124 cells) of intravasated tumor cells compared to control (2 out of 304 cells), suggesting that TNF-α stimulation increased endothelial permeability (Fig. S1*C*) and enhanced intravasation rate (Fig. S3*A*). Moreover, to characterize the TNF-α-induced endothelial barrier disruption in detail we measured permeability at different doses of TNF-α (0, 0.2, 2 and 20 ng/mL) and observed a graded response in endothelial permeability (Fig. S1*A*).

We further investigated the role of endothelial permeability in tumor-endothelial interactions during tumor cell invasion. Here, we used a highly invasive human fibrosarcoma (HT1080) cell line, in the absence of macrophages. To facilitate analysis, we developed a quantification framework that enabled the automatic detection (*SI Materials and Methods*) of tumor-endothelial interaction events, defined as a tumor cell in direct physical contact with the endothelial monolayer. This event can occur in the endothelial channel, or on the ECM-endothelial channel interface after migration of the tumor cell from the 3D matrix toward the endothelial barrier. Fig. 4 *A* and *B* show two confocal image 3D volume renderings at $t = 0$ and $t = 10$ h of the HT1080 fibrosarcoma cells inside the 3D matrix as they invade toward the endothelial monolayer. The number of tumor cells that had migrated beyond the ECM-endothelial channel interface (Fig. 4 *C* and *D*) increased with time, as the tumor cells were migrating in response to the EGF gradient toward the endothelium. Stimulation of the endothelium with 2 ng/mL TNF-α resulted in a 1.7-fold ($P = 0.006$) increase in percentage of tumor cells that interacted with the endothelium compared to the control (Fig. 4*E*). We confirmed that at $t = 0$ h, prior to tumor cell migration toward the endothelium, the number of tumor cells located within 250 μm from the ECM-endothelial channel interface was similar between the two conditions (Fig. S3*B*).

In addition to changes in the number of tumor-endothelial interaction events, the TNF-α stimulated endothelium showed a fivefold increase ($P = 0.002$) in endothelial permeability compared to the control (Fig. 4*F*). Real-time measurements of $P_D$ also confirmed the endothelial barrier impairment for 10 and 70 kDa dextrans (Fig. S1*A*). The TNF-α concentration (2 ng/mL) used was determined by titration experiments on endothelial monolayers seeded on collagen hydrogels to ensure a confluent endothelial monolayer was present after 24 h of stimulation (*SI Materials and Methods* and Fig. S3*C*).

**Characterization of Macrophage Polarization and Role of Macrophage-Secreted TNF-α in Regulating Tumor Cell Intravasation and Endothelial Barrier Function.** To characterize whether macrophages were polarized in the microfluidic device, we performed immunostaining for M1 and M2 markers (*SI Materials and Methods* and

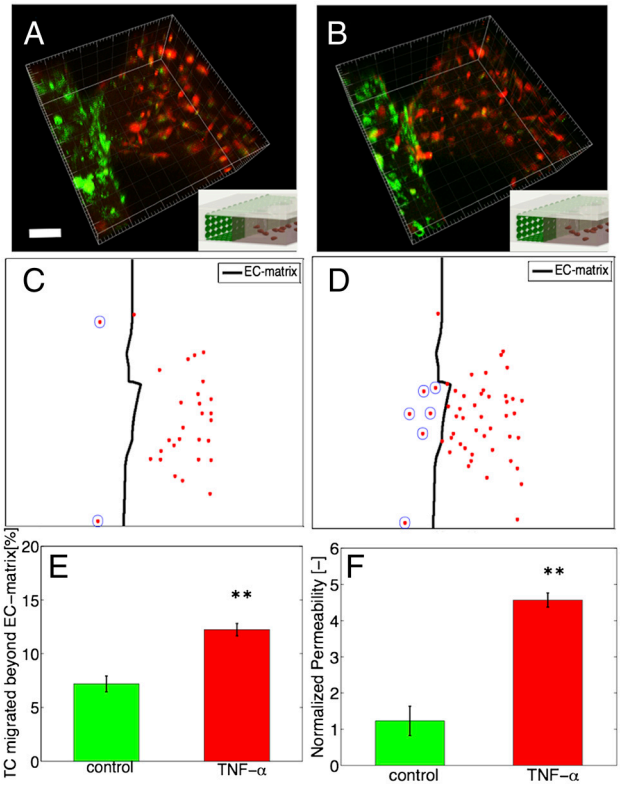


**Fig. 4.** TNF-α effects on tumor-endothelial interactions and endothelial permeability. (*A* and *B*) Three-dimensional rendering of a single hydrogel region showing fibrosarcoma tumor cells (HT1080, red) next to endothelial monolayer (MVEC, green) at time $t = 0$ h (*A*) and $t = 10$ h (*B*). *Inset* shows image orientation in the device. (Scale bar: 50 μm.) (*C* and *D*) Projected confocal slices showing all tumor cells (red dots) located within 250 μm from the 3D ECM-endothelial channel interface (outlined with a thick black line) at $t = 0$ h (*C*) and $t = 10$ h (*D*). (Scale bar: 50 μm.) (*E*) Percentage of tumor cells that interacted with the endothelium to the total cells in the hydrogel region ($P = 0.006$). Average values ($n = 3$ devices) for each condition. (*F*) Normalized change in permeability after 10 h, for the control and TNF-α conditions ($P = 0.002$). Average values for at least $n = 10$ hydrogel regions; error-bars represent SEM.

Fig. S4). Although we found that macrophages within the device could be driven toward an M1 or M2 phenotype through stimulation with lipopolysaccharide (LPS) or interleukin-4 (IL4) (Fig. S4*C*), respectively, when in the presence of tumor cells and endothelial cells the macrophages were variable in their expression for M1 or M2-specific markers (Fig. S4 *D* and *E*). Furthermore, coculture of macrophages with tumor cells within the device did not significantly change their phenotype vs. culture of macrophages alone (Fig. S4 *D* and *E*). We also characterized macrophage-secreted factors under control conditions and M1/M2 polarization and confirmed that the macrophages secreted TNF-α (Fig. S4 *A* and *B*).

To investigate whether the effects of macrophages on intravasation and endothelial permeability are regulated via paracrine signals, we performed antibody blocking experiments to neutralize soluble TNF-α and measured significant changes in permeability (Fig. 3*E*, 1.67-fold decrease, $P = 0.04$) and intravasation (Fig. 3*D*, 2.45-fold decrease, $P = 0.03$) compared to control IgG antibody. We also performed permeability measurements to investigate the effects of other cell types (tumor and epithelial cells) on endothelial barrier function compared to macrophages. Interestingly, the presence of all cell types resulted in increased endothelial permeability (Fig. S2*D*) compared to the control condition. However, the presence of macrophages resulted in a significant increase in $P_D$ compared to tumor cells ($5.6 \times 10^{-5}$ cm/s vs. $3.9 \times 10^{-5}$ cm/s, $P = 0.049$), whereas there was no significant difference compared to the epithelial cell ($5.6 \times 10^{-5}$ cm/s vs. $4.5 \times 10^{-5}$ cm/s, $P = 0.36$) condition.

**Dynamics of Tumor-Endothelial Cell Interactions.** Our ability to visualize the endothelium en face allows a qualitative characterization of the process of tumor cell migration at a 3D endothelial monolayer with a well-defined lumen (Fig. 1*C*). Such dynamic observation of tumor-endothelial cell interactions can offer valuable insights into the timescales, spatial organization, and mechanism of tumor cell intravasation, complementary to detailed immunofluorescent staining (Fig. 3*A* and Fig. S5). Fig. 5*A* shows a time series of images demonstrating one example of a fibrosarcoma cell migrating from the 3D matrix to the endothelial monolayer. Analysis of the time-lapse movies led to a number of interesting observations: (*i*) Invasive protrusions form dynamically and appear to probe the surrounding 3D environment. (*ii*) Tumor cells exhibit significant cell shape changes as they migrate from the 3D matrix, adhere to the endothelium, and migrate through it to the endothelial channel. (*iii*) Tumor cells were observed to migrate toward remodeled regions (Fig. S5) of the endothelium or next to a macrophage (Fig. S2*C*).

We studied the dynamic interactions of tumor-endothelial cells under control and TNF-α conditions by tracking tumor cell trajectories (Fig. 5*B*) and quantifying the time (Fig. 5*C*) required for tumor cells to migrate a specific distance (60 μm) across the ECM-endothelial channel interface. Tumor cells migrated faster from the 3D matrix into the endothelial channel in the TNF-α stimulated ($1.35 \pm 0.25$ h) compared to the control monolayer ($2.42 \pm 0.38$ h) ($P = 0.024$). To confirm that TNF-α did not modulate tumor cell invasion in the 3D matrix, we quantified tumor cell migration speeds (Fig. 5*D*) and found similar values ($29.59 \pm 2.57$ vs. $29.53 \pm 4.16$ μm/h, $P = 0.99$) under the two conditions. These findings suggest that impaired endothelial barrier function facilitates faster tumor cell invasion across the

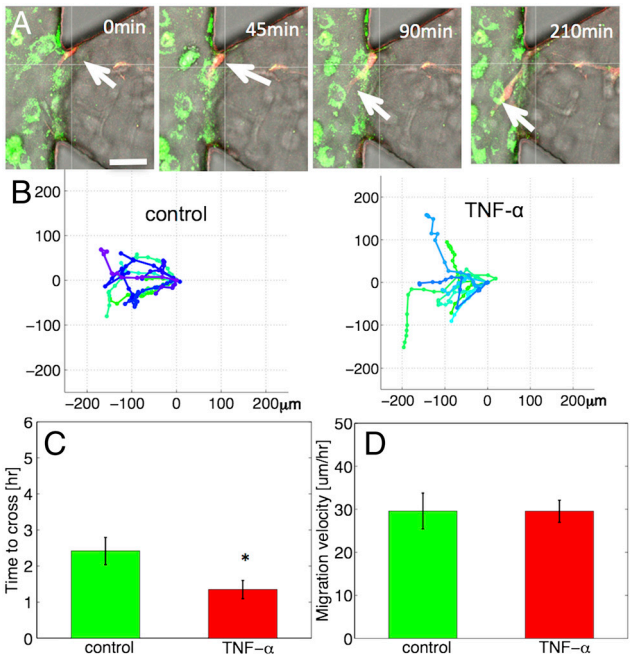


**Fig. 5.** Dynamics of tumor-endothelial interactions. (*A*) Time series of confocal images showing a HT1080 cell (red, white arrow) invading toward the TNF-α stimulated endothelial monolayer (MVEC, green). (Scale bar: 50 μm.) (*B*) Tumor cell trajectories over 10 h under control (*Left*) and TNF-α conditions (*Right*). (*C*) Time required for tumor cells to migrate over a 60 μm distance across the EC-matrix ($P = 0.02$). (*D*) Mean migration speed of HT1080 cells in the 3D matrix ($P = 0.99$). Average values for at least $n = 10$ trajectories per condition in *A–D*; error-bars represent SEM.

EC-matrix barrier and are in agreement with our observations of increased endothelial permeability and higher number of tumor cells interacting with the TNF-α stimulated endothelium.

## Discussion

Despite progress in identifying critical regulators (16, 30–32) of tumor-endothelial interactions, it is not clear whether tumor cell entry into the blood stream requires an impaired endothelial barrier (30, 33). In this work, we present a unique approach using a microfluidic-based in vitro assay that enables real-time visualization and quantification of the interactions between tumor cells and an endothelial monolayer in the context of tumor cell invasion and intravasation. Because tumor blood vessels are structurally (18) and functionally (19) abnormal, we hypothesized that endothelial barrier function impairment contributes to tumor cell intravasation. We found that modulation of endothelial barrier permeability by added soluble biochemical factors, such as TNF-α, and via macrophages can facilitate intravasation, and regulate the number and dynamics of tumor-endothelial cell interactions. Our findings are consistent with in vivo observations of high tumor cell counts in the portal venous blood in metastatic tumors with higher blood vessel density (34) and with a study that demonstrated that vascular endothelial growth factor (VEGF) overexpression by tumor cells induced endothelial barrier disruption and facilitated transendothelial migration (32).

Previous studies of cancer cell intravasation have largely taken a cancer cell-centric approach identifying signaling pathways that increase tumor cell dissemination (9–11). For example, a recent in vitro study identified changes in endothelial myosin light chain kinase upon tumor-endothelial cell contact (16), however this method did not allow for measurement of endothelial permeability or the accurate control of the microenvironmental stimuli. Compared to other in vitro models (16, 21) and microfluidic models of tumor-endothelial interactions (25, 35), our assay provides a number of unique features, such as high-resolution live cell imaging, the formation of an endothelial monolayer on a 3D ECM enabling us to model intravasation, and for precise quantification and control of critical tumor microenvironmental factors. The readily accessible apical side of the endothelium allows for the introduction of cell types in the tumor microenvironment, such as macrophages, the precise establishment of growth-factor gradients, fluid flow, and real-time spatially resolved endothelial barrier function measurements. All three cell types (tumor, endothelial, macrophages) can interact in a 3D environment with an ECM which can be remodeled by cells, enabling autocrine, paracrine, and juxtracine cell-cell interactions mimicking the angiogenic tumor microenvironment (17) more faithfully than studies on two-dimensional substrates (36).

Endothelial barrier function quantitation in the presence of invading cells showed size-selective transendothelial transport and the $P_D$ values in our microfluidic model agree well with measurements in transwell systems (37) and in engineered blood vessels in 3D matrices (38). Although our measurements are significantly higher than in vivo values of healthy vasculature (39), they are of the same order of magnitude (Fig. 2*C*, $P_D \sim 10^{-6}$ cm/s) as those measured in murine tumors with 70 kDa dextran (40). Contrary to the traditional transwell method that provides only a single $P_D$ value across the entire monolayer, our approach allows for (*i*) detailed regional investigation of endothelial permeability changes in response to tumor-stromal cell interactions and (*ii*) the accurate measurement of the endothelial permeability dynamics (in cm/s) for direct comparison between different studies.

The ability to image the tumor-endothelial cell dynamics in high-resolution allowed us to visualize the diverse array of tumor cell phenotypes: 3D invasion in response to growth factor gradients, direct physical contact with, and migration on an endothelial monolayer. Detailed single tumor cell tracking was performed to quantify the timescales of tumor-endothelial cell interactions in the context of intravasation. We found that these timescales and the number of tumor cells interacting with the endothelium were dependent on endothelial barrier function. Under conditions of unperturbed endothelial barrier function, carcinoma cells were observed predominantly on the basal endothelial side, whereas increased permeability facilitated intravasation and enhanced the number of tumor-endothelial interactions. Our results agree with in vivo studies in a zebrafish model (10) that found increased intravasation by tumor cells that overexpressed angiogenic growth factors, with studies in murine models (9, 12), and in clinical specimens (41) that demonstrated macrophage-assisted intravasation. Interestingly, our measured timescales of tumor cell migration across the EC-matrix interface (Fig. 5*C*) in the device are comparable to in vivo measurements (12). The measured increase in intravasation rate associated with the presence of macrophages (Fig. 3*E*) may also be facilitated by the EGF/colony stimulating factor 1 (CSF-1) paracrine loop between tumor cells and macrophages, leading to enhanced tumor cell invasiveness (42). In the absence of macrophages the TNF-α-induced intravasation rate enhancement (Fig. S3*A*) may also involve proinvasive effects of TNF-α on the tumor cells (43). Moreover, blocking antibody experiments demonstrated an important role for macrophage-secreted TNF-α (Fig. 3*E*), increasing endothelial permeability in the presence of macrophages. Interestingly, blocking TNF-α did not reduce intravasation to baseline levels, suggesting that there may be additional macrophage-secreted factors or juxtacrine interactions that facilitate intravasation. Permeability experiments with tumor and epithelial cells in place of macrophages (Fig. S2*D*) showed that although all cell types resulted in increased permeability values macrophages are the most potent. The measured permeability increases for the tumor and epithelial cells may be facilitated via secretion of angiogenic factors such as VEGF (44). Our observations of enhanced tumor cell intravasation rate and tumor-endothelial interactions may also be linked to physical remodeling of the endothelial barrier. Through immunofluorescence imaging we observed that at locations of tumor-endothelial cell contact the VE-cadherin junctions appear remodeled (Fig. S5) in agreement with other studies (31). Finally, although we could polarize macrophages in an M1 or M2 state in the device through LPS or IL4 stimulation (Fig. S4*C*), the macrophages were variable in their expression of M1 and M2 marker during coculture conditions, forming a mixed and heterogeneous population similar to in vivo (45).

In summary, we present a microfluidic-based approach to investigate tumor cell intravasation through the integration of high-resolution live imaging with endothelial barrier function measurement in the presence of macrophages. Also, by virtue of the small amounts of reagents and cells needed, and the capability to embed clinical tissue in the 3D ECM, our microfluidic model may find applications in personalized medicine, enabling economical drug screening and discovery integrating two or more cell types. Here, we characterize the previously unexplored timescales of tumor-endothelial cell interactions during intravasation and demonstrate the interplay of endothelial permeability and tumor-endothelial signaling. The ability to model the interactions of invading cells with an endothelium in a 3D microenvironment also offers the possibility to study the interplay of endothelial barrier function and transendothelial migration in other physiological and pathological processes, such as immune cell trafficking and cancer cell extravasation.

## Materials and Methods

**Cell Culture, Staining, and Reagents.** The human fibrosarcoma HT1080 [American Type Culture Collection (ATCC)] and breast carcinoma MDA231 overexpressing GFP-tagged MenaINV (Gertler Lab) cell lines were cultured in DMEM supplemented with antibiotics and 10% FBS (Invitrogen) and grown until 70% confluence. Primary MVEC (Lonza) and macrovascular endothelial cells (HUVEC; Chan Lab, National University of Singapore, Singapore) were grown in Endothelial cell medium (EGM2-MV) (Lonza) to confluence. For

the intravasation studies, we used the murine macrophage cell line RAW264.7 (ATCC) cultured in DMEM supplemented with 10% heat inactivated FBS.

**Microfluidic Device Design.** The microfluidic device design is based on previous work from our lab on forming endothelial sprouts under growth-factor gradients and the fabrication protocols are described in detail elsewhere (46). Compared with previous microfluidic systems from our group, two unique characteristics of the present design are (*i*) the incorporation of a *y*-junction for precise control of concentration gradients, required for accurate measures of endothelial permeability and (*ii*) the high number ($n = 37$) of hydrogel ECM regions (Fig. 1*B*).

**Endothelial Barrier Function Characterization.** We developed a quantitative framework to measure the local diffusive permeability ($P_D$) of the endothelial monolayer using fluorescent dextrans and an analytical model based image analysis (see *SI Materials and Methods* for details and data analysis).

**Tumor-Endothelial Cell Interactions Assay.** HT1080 cells were seeded in the tumor channel and were allowed to invade for 3 d into the 3D ECM, when, a confluent endothelial monolayer was formed on the 3D ECM-endothelial channel. Prior live cell imaging was performed an EGF gradient and TNF-α stimulation were applied. Images were analyzed using Imaris (Bitplane) to identify the ECM-endothelial channel interface and track tumor cell centroids (see *SI Materials and Methods* for detailed methods and data analysis).

**Tumor Cell Intravasation Assay.** Breast carcinoma cells were seeded in the presence or absence of macrophages inside the 3D ECM and after 24 h an endothelial monolayer was formed. EGF gradients were established in all experiments and cells were allowed to interact for 48 h, after which fixation, staining, and imaging were performed (see *SI Materials and Methods* for detailed methods and data analysis).

**ACKNOWLEDGMENTS.** We acknowledge Dr. Joan Brugge and Dr. Jean-Paul Thiery for helpful discussions, Dr. Seok Chung for establishing earlier microfluidic coculture assays in the Kamm Lab and Dr. Ron Weiss for kindly allowing us access to the confocal microscope facilities of his lab. Funding from National Cancer Institute R21CA140096 (to J.L.C., R.D.K.), CA100324 (to J.S.C), National Institutes of Health Grant GM58801 (to F.B.G.), CDMRP Department of Defense Breast Cancer Research Program Grant W81XWH-10-1-0040 (to S.K.H.-A), and wafer fabrication facilities at Microsystems Technology Laboratory (Cambridge, MA) are greatly appreciated.

1. Nguyen DX, Bos PD, Massague J (2009) Metastasis: From dissemination to organ-specific colonization. *Nat Rev Cancer* 9:274–284.
2. Steeg PS (2006) Tumor metastasis: Mechanistic insights and clinical challenges. *Nat Med* 12:895–904.
3. Friedl P, Alexander S (2011) Cancer invasion and the microenvironment: Plasticity and reciprocity. *Cell* 147:992–1009.
4. Quigley JP, Armstrong PB (1998) Tumor cell intravasation alu-cidated: The chick embryo opens the window. *Cell* 94:281–284.
5. Roussos ET, Condeelis JS, Patsialou A (2011) Chemotaxis in cancer. *Nat Rev Cancer* 11:573–587.
6. Calvo F, Sahai E (2011) Cell communication networks in cancer invasion. *Curr Opin Cell Biol* 23:621–629.
7. Joyce JA, Pollard JW (2009) Microenvironmental regulation of metastasis. *Nat Rev Cancer* 9:239–252.
8. Giampieri S, et al. (2009) Localized and reversible TGFbeta signaling switches breast cancer cells from cohesive to single cell motility. *Nat Cell Biol* 11:1287–1296.
9. Roussos ET, et al. (2011) Mena invasive (MenaINV) promotes multicellular streaming motility and transendothelial migration in a mouse model of breast cancer. *J Cell Sci* 124:2120–2131.
10. Stoletov K, Montel V, Lester RD, Gonias SL, Klemke R (2007) High-resolution imaging of the dynamic tumor cell vascular interface in transparent zebrafish. *Proc Natl Acad Sci USA* 104:17406–17411.
11. Zijlstra A, Lewis J, Degryse B, Stuhlmann H, Quigley JP (2008) The inhibition of tumor cell intravasation and subsequent metastasis via regulation of in vivo tumor cell motility by the tetraspanin CD151. *Cancer Cell* 13:221–234.
12. Wyckoff JB, et al. (2007) Direct visualization of macrophage-assisted tumor cell intravasation in mammary tumors. *Cancer Res* 67:2649–2656.
13. Bekes EM, et al. (2011) Tumor-recruited neutrophils and neutrophil TIMP-free MMP-9 regulate coordinately the levels of tumor angiogenesis and efficiency of malignant cell intravasation. *Am J Pathol* 179:1455–1470.
14. Gupta GP, Massague J (2006) Cancer metastasis: Building a framework. *Cell* 127:679–695.
15. Bockhorn M, Jain RK, Munn LL (2007) Active versus passive mechanisms in metastasis: Do cancer cells crawl into vessels, or are they pushed? *Lancet Oncol* 8:444–448.
16. Khuon S, et al. (2010) Myosin light chain kinase mediates transcellular intravasation of breast cancer cells through the underlying endothelial cells: A three-dimensional FRET study. *J Cell Sci* 123:431–440.
17. Hagendoorn J, et al. (2006) Onset of abnormal blood and lymphatic vessel function and interstitial hypertension in early stages of carcinogenesis. *Cancer Res* 66:3360–3364.
18. Hashizume H, et al. (2000) Openings between defective endothelial cells explain tumor vessel leakiness. *Am J Pathol* 156:1363–1380.
19. Nagy JA, et al. (2006) Permeability properties of tumor surrogate blood vessels induced by VEGF-A. *Lab Invest* 86:767–780.
20. Kedrin D, et al. (2008) Intravital imaging of metastatic behavior through a mammary imaging window. *Nat Methods* 5:1019–1021.
21. Li YH, Zhu C (1999) A modified Boyden chamber assay for tumor cell transendothelial migration in vitro. *Clin Exp Metastasis* 17:423–429.
22. Zervantonakis IK, et al. (2010) Concentration gradients in microfluidic 3D matrix cell culture systems. *Int J Micro-Nano Scale Transp* 1:27–36.
23. Abhyankar VV, et al. (2008) A platform for assessing chemotactic migration within a spatiotemporally defined 3D microenvironment. *Lab Chip* 8:1507–1515.
24. Huang CP, et al. (2009) Engineering microscale cellular niches for three-dimensional multicellular co-cultures. *Lab Chip* 9:1740–1748.
25. Song JW, et al. (2009) Microfluidic endothelium for studying the intravascular adhesion of metastatic breast cancer cells. *PLoS One* 4:e5756.
26. Hwang YP, et al. (2011) Suppression of EGF-induced tumor cell migration and matrix metalloproteinase-9 expression by capsaicin via the inhibition of EGFR-mediated FAK/Akt, PKC/Raf/ERK, p38 MAPK, and AP-1 signaling. *Mol Nutr Food Res* 55:594–605.
27. Price JT, Tiganis T, Agarwal A, Djakiew D, Thompson EW (1999) Epidermal growth factor promotes MDA-MB-231 breast cancer cell migration through a phosphatidylinositol 3′-kinase and phospholipase C-dependent mechanism. *Cancer Res* 59:5475–5478.
28. Condeelis J, Pollard JW (2006) Macrophages: Obligate partners for tumor cell migration, invasion, and metastasis. *Cell* 124:263–266.
29. Lohela M, Werb Z (2010) Intravital imaging of stromal cell dynamics in tumors. *Curr Opin Genet Dev* 20:72–78.
30. Mierke CT (2011) Cancer cells regulate biomechanical properties of human microvascular endothelial cells. *J Biol Chem* 286:40025–40037.
31. Peng HH, Dong C (2009) Systemic analysis of tumor cell-induced endothelial calcium signaling and junction disassembly. *Cell Mol Bioeng* 2:375–385.
32. Weis S, Cui J, Barnes L, Cheresh D (2004) Endothelial barrier disruption by VEGF-mediated Src activity potentiates tumor cell extravasation and metastasis. *J Cell Biol* 167:223–229.
33. Mierke CT (2008) Role of the endothelium during tumor cell metastasis: Is the endothelium a barrier or a promoter for cell invasion and metastasis? *J Biophys* 2008:183516.
34. Tien YW, et al. (2001) Tumor angiogenesis and its possible role in intravasation of colorectal epithelial cells. *Clin Cancer Res* 7:1627–1632.
35. Zheng C, et al. (2012) Quantitative study of the dynamic tumor-endothelial cell interactions through an integrated microfluidic coculture system. *Anal Chem* 84:2088–2093.
36. Stine MJ, et al. (2011) Integration of genotypic and phenotypic screening reveals molecular mediators of melanoma-stromal interaction. *Cancer Res* 71:2433–2444.
37. Albelda SM, et al. (1988) Permeability characteristics of cultured endothelial cell monolayers. *J Appl Physiol* 64:308–322.
38. Chrobak KM, Potter DR, Tien J (2006) Formation of perfused, functional microvascular tubes in vitro. *Microvasc Res* 71:185–196.
39. Michel CC, Curry FE (1999) Microvascular permeability. *Physiol Rev* 79:703–761.
40. Dreher MR, et al. (2006) Tumor vascular permeability, accumulation, and penetration of macromolecular drug carriers. *J Natl Cancer Inst* 98:335–344.
41. Robinson BD, et al. (2009) Tumor microenvironment of metastasis in human breast carcinoma: A potential prognostic marker linked to hematogenous dissemination. *Clin Cancer Res* 15:2433–2441.
42. Patsialou A, et al. (2009) Invasion of human breast cancer cells in vivo requires both paracrine and autocrine loops involving the colony-stimulating factor-1 receptor. *Cancer Res* 69:9498–9506.
43. Montesano R, Soulie P, Eble JA, Carrozzino F (2005) Tumour necrosis factor alpha confers an invasive, transformed phenotype on mammary epithelial cells. *J Cell Sci* 118:3487–3500.
44. Lee TH, Avraham HK, Jiang S, Avraham S (2003) Vascular endothelial growth factor modulates the transendothelial migration of MDA-MB-231 breast cancer cells through regulation of brain microvascular endothelial cell permeability. *J Biol Chem* 278:5277–5284.
45. Mantovani A, Sica A, Locati M (2007) New vistas on macrophage differentiation and activation. *Eur J Immunol* 37:14–16.
46. Sudo R, et al. (2009) Transport-mediated angiogenesis in 3D epithelial coculture. *FASEB J* 23:2155–2164.